RSC Advances

ROYAL SOCIETY OF CHEMISTRY

www.rsc.org/advances

Homogenously Magnetically Concentrated Silver Nanoparticles for Uniform "Hot Spots" in Surface Enhanced Raman Spectroscopy

Andrew J Frank, Alanna McEneny-King, Nicole Cathcart and Vladimir Kitaev*

Department of Chemistry and Biochemistry, Wilfrid Laurier University,

75 University Avenue W., Waterloo, Ontario, Canada

ABSTRACT

We report reproducible and sensitive surface-enhanced Raman spectroscopy (SERS) detection achieved with a developed nanoparticle platform, Ag&MH. Ag&MH is comprised of silver nanoparticles (AgNPs), as a sensing substrate that is efficiently and uniformly magnetically concentrated with the assistance of maghemite, γ-Fe_2O_3, nanoparticles (MHNPs). MNHPs were optimized synthetically for minimal charge interactions with AgNPs and low optical absorbance. At sufficiently high concentrations, magnetic maghemite NPs hydrodynamically trap AgNPs and concentrate them on the inner surface of a quartz optical cell to form an Ag&MH SERS substrate for highly reproducible SERS detection. The reproducibility is a combination of several factors contributing to uniform "hot spots": homogeneous magnetic concentration by gentle hydrodynamic trapping and weak electrostatic interactions of the same-charge nanoparticles and non-close packing of AgNPs, in particular decahedra. Size-uniform silver decahedra nanoparticles (AgJ_{13}NPs) featuring sharp localized surface plasmon resonance (LSPR) peaks, coupled with minimized optical interference from MHNPs, enable sensitive and reproducible SERS detection, where 5,5'-dithiobis-(2-nitrobenzoic acid), DTNB, was used as a probe molecule. Reproducibility of independent measurements at nanomolar level was ca. 10% – consistently overcoming the "hot spot" problem through uniform distribution of AgJ_{13}NPs in the Ag&MH SERS substrate. Picomolar concentrations were detected using a simple fiber-optic Raman spectrometer. The developed AgJ_{13}&MH sensing platform is promising for convenient and reproducible SERS detection of analytes in common laboratory settings.

* E-mail: vkitaev@wlu.ca

INTRODUCTION

Plasmonic metal nanoparticles (MNPs)[1] demonstrate excellent potential for applications in sensing[23-6] and diagnostics.[2,7,8,9] owing to their unique optical properties tuneable by size and shape.[10,11] One of the most established and researched sensing methods utilizing plasmonic NPs is SERS.[6,12] SERS is a sensitive technique for the identification of a variety of analytes.[4,13] LSPR of noble metal NPs is well documented and established for enhancing the Raman scattering cross-sections of adsorbed molecules;[14,15] silver especially has been used for SERS since the early 1970's.[16]

Efficiency and utility of noble metal nanoparticles as SERS substrates can be further enhanced by incorporating magnetic separation.[17-22] A combination of silver NPs with magnetic NPs has been shown to be advantageous for a wide range of potential applications by utilizing the SERS ability of silver NPs and the magnetic field controllability of superparamagnetic NPs.[23,24] Notable biochemical applications include silver NPs affixed to polystyrene coated magnetite NPs for protein separation and identification,[25] sensitive detection of DNA,[26] and silver-silica core-shell NPs affixed to magnetite for separation in immunoassays using SERS for identification.[27] One example of the biochemical applications is a SERS-based sandwich immunoassay that employs immunomagnetic separation to concentrate *Escherichia coli* (*E. coli*) cells.[28]

The magnetic component enables efficient concentration of a small amount of analyte, resulting in improved detection limits, as well as a higher density of Raman active "hot spots".[29-32] Improved SERS detection limits are common for magnetic silver NP systems.[33-37] Silver-coated magnetite NPs have been demonstrated to serve as an effective analysis tool for SERS of organic molecules such as naphthalene,[38] with an important advantage being ease of separation for recycling of the SERS-active NPs for subsequent Raman analysis.[39]

One of the major limitations in SERS measurements with nanoparticle substrates, including magnetic systems, is the reproducibility dealing with "hot spots" for the reliable detection.[2,3] Intense research efforts were directed to address the

reproducibility of "hot spots",[40,41] which still remains a problem for the use of regular non-modified nanoparticles as a SERS substrate.[42]

Herein we present an effective SERS detection platform composed of maghemite and silver decahedral NPs (AgJ_{13}NP&MH), which enables a high degree of reproducibility in SERS detection and picomolar detection limits. AgJ_{13}NP&MH utilizes a combination of two simple independent components, where maghemite NPs carry the same charge as AgNPs to interact gently with AgNPs and to uniformly concentrate AgJ_{13}NPs with the adsorbed analyte upon application of magnetic field. Together with a uniform AgNP concentration, low optical absorption of magnetite and sharp LSPR peaks of AgJ_{13}NP enable sensitive SERS detection. AgJ_{13}&MH can be conveniently prepared by an environmentally friendly all-aqueous synthetic procedure and can serve as a versatile SERS substrate, with notable advantages of high reproducibility and low detection limits.

EXPERIMENTAL

Reagents

For all experiments, high purity deionized water (>18.3 MΩ·cm) was produced by a Millipore A10 Milli-Q system. Iron (II) perchlorate hydrate (98%), L-arginine (98%), silver nitrate (99+%), hydrogen peroxide (99.999%) 30 wt.% in water, sodium citrate tribasic dihydrate (99.0%), sodium borohydride (99%), and 5,5'-dithiobis-(2-nitrobenzoic acid) (99%) were supplied by Sigma-Aldrich. Poly(vinylpyrollidone) with average M_w of 40,000 (99.0%) was supplied by Caledon. Argon (PP 4.8) was provided by Praxair. All chemicals were used as received.

Synthesis

Monodisperse silver decahedral nanoparticles (AgJ_{13}NPs), 45 ± 3 nm across the pentagonal rim (Fig. S4), were prepared as previously reported in the original procedure,[43] and aged a minimum of ten days to ensure decomposition of any unreacted sodium borohydride and hydrogen peroxide.

Magnetite (Fe_3O_4) was synthesized following a modified one-pot aqueous synthesis.[44] In a typical preparation, 200 µL of 0.2 M arginine was added to 8.4 mL of deionized water in a 20 mL borosilicate vial (VWR) sealed with a rubber septum. The solution was sonicated and deoxygenated. Under argon gas flow, 1.00 mL of similarly deoxygenated 0.026 M iron (II) perchlorate was added to the arginine solution via syringe to attain a 1:1 molar ratio between arginine and iron (II). The gas flow was removed and the septum-sealed vial was left to react at room temperature overnight. The reaction solution started olive green and slowly turned brown in several hours, and then gradually a black precipitate of arginine-stabilized magnetite nanoparticles formed.

Maghemite (γ-Fe_2O_3, an oxidized form of magnetite) was prepared by combining 2.50 mL of 0.2 M arginine, 1.25 mL of 0.026 M iron (II) perchlorate and 8.25 mL of deionized water. Initially a deep olive dispersion, a medium brown magnetic precipitate forms within 3-5 hours in an open vial.

SERS sample preparation

The composite dispersions of magnetic and plasmonic NPs for SERS experiments were prepared by first concentrating 12.0 mL of the as prepared AgJ_{13}NP dispersion by centrifugation and redispersing it in 7.5 mL of high purity deionized water. To this dispersion, 188 µL of 0.1 M poly(vinylpyrollidone) (PVP) was added, for an overall PVP concentration of 2.5 mM. Either magnetite or maghemite nanoparticle dispersions were then added to the redispersed AgJ_{13}NP solution to produce iron-to-silver ratios ranging from 0.25:1 to 5:1. For a typical 1:1 iron-to-silver preparation, 100 µL of the as prepared maghemite dispersion (2.7 mM iron concentration) was added to 1.25 mL of the redispersed AgJ_{13}NP solution (0.20 mM silver concentration) and diluted with deionized water to a final volume of 2.50 mL. Composite dispersions of other plasmonic nanoparticles were prepared according to a similar protocol. Optimal equilibration time for the composite dispersions prior to SERS measurements is 4 to 12 hours. The samples remain functional for at least 3-4 days after mixing.

For SERS measurements, samples were prepared by transferring 0.625 mL of the above prepared composite dispersion to a 0.5 cm quartz cell. After the analyte solution was

introduced, the cell was shaken mechanically for 5-10 seconds then positioned next to a 5-mm circular rare earth magnet to form a compact deposit on an inner wall of the quartz cell for SERS measurements, see measurement schematics in Figure 1a. The laser beam of the Raman probe was centered on these composite deposits to yield highly reproducible Raman measurements with low detection limits. The SERS analyte was 5,5'-dithiobis-(2-nitrobenzoic acid), DTNB. Measurements could be also performed in PMMA cells. For those measurements, a liquid cap (see below) was used to make the measurements from the back side of the cell, so the material of the cell would not interfere.

Characterization

Raman spectroscopy was performed using a R-3000QE fiber-optic Raman spectrometer equipped with a 290 mW laser at 785 nm (RSI), operated at 190 mW with 5 second integration time (see Fig. S8-S10and Table S3 for the selection of optimal laser power and integration times). Both solid cap and liquid caps were used that focus the probing beam on the cell's surface and inside the cell, respectively. Focusing the beam inside the cell with the liquid cap enabled measurements from the inner surface of the pellet. Visible spectroscopy was carried out using either an Ocean Optics QE-65000 fiber-optic UV-vis spectrometer or a Cary 50 Bio UV-vis spectrophotometer. Electron microscopy (EM) imaging, both transmission (TEM) and scanning (SEM), was performed using a Hitachi S-5200 with a typical operating voltage of 30.0 kV. The samples were deposited onto a copper grid with a formvar/carbon film (FCF-200, EMS Corp.). Zetasizer S (Malvern Instruments) was used to measure both zeta potentials and to estimate hydrodynamic particle sizes. PXRD measurements were performed using D2 Phaser diffractometer (141 mm goniometer radius) with Cobalt radiation (30 kV, 10 mA), LYNXEYE silicon strip detector, and iron K-beta filter. Samples were prepared by drop-casting onto a low-background silicon wafer and allowed to dry prior to measurements. Signal was collected for 3 hours. Quantitative Rietveld refinement was performed using an approach based on fundamental parameters with DIFFRAC.TOPAS and crystallographic structures exported from the ICDD PDF-4 Database (Release 2014).

RESULTS AND DISCUSSION

Preparation of Ag&MH SERS substrate.

The experimental protocol of SERS measurements with Ag&MH is summarized schematically in Figure 1a. The analyte, DTNB, was reproducibly detected by SERS using a composite substrate of AgJ_{13}NPs and maghemite NPs (AgJ_{13}NP&MH) formed by magnetic concentration. Magnetic NPs were concentrated by a strong permanent magnet, and at sufficiently high concentrations (starting with 0.05 mM of maghemite – see Figs. S1 and S2 and Table S2) were able to hydrodynamically drag AgJ_{13}NPs and uniformly concentrate them. The image of the pellet is shown in Fig. S3d. As a result, the AgJ_{13}NP&MH substrate was built on the inner wall of the quartz cell within a few minutes (typically 3-5 minutes, see Fig. 2d). The deposited AgJ_{13}NP&MH layer remained intact after the magnet was removed (Fig. S3d). As a SERS substrate, AgJ_{13}NP&MH enables remarkable measurement reproducibility: both for different samples areas within the same substrate and upon subsequent dispersal and re-deposition of the substrate film (see right panel of Fig. 1a for a representative spectrum and Table S1 for the data). Effectively, very uniform hot spots were created in the AgJ_{13}NP&MH substrate by virtue of the low size-dispersity of AgJ_{13}NPs and homogenous deposition of AgNPs.

Key features of Ag&MH

Maghemite. The use of maghemite is essential due to several factors. First is its weaker optical absorption compared to magnetite (Fig. 2c), which is crucial for the sensitivity of detection. The maghemite preparation was optimized to achieve smallest uniform particles (ca. 4-5 nm) with the least optical absorption (Figs. 1b,c). Since Fe(II) was used as a starting precursor, uniform oxidation of most of Fe(II) to Fe(III) was required to achieve minimized optical absorption. Typically the optimal properties have been reached after 3-5 hours, in line with the recent report on maghemite formation.[45] The maghemite samples typically contain some residual magnetite. For the larger-scale sample (0.5 g of maghemite) prepared for PRXD, the amount of magnetite can be interpolated from the deconvolution process of the very close magnetite and

maghemite peaks, as 30±2 vol.% (Fig. S7). The large-scale sample was oxidized less efficiently, so the amount of actual maghemite component in typical AgJ_{13}NP&MH samples is likely less. An important factor, again, is appreciably less absorbance of AgJ_{13}NP&MH samples (Figs. 1b,c).

The second important factor is the same surface charges of magnetic and plasmonic NPs required to avoid strong electrostatic interactions of nanoparticles and their irreversible aggregation. The weakly negative surface charge of MHNPs (zeta potential of -9 mV) was achieved using excess of arginine as a capping ligand. The negative charge of MHNPs is corroborated by the maximum colloidal stability at weakly basic pH of ca. 8 (Fig. S11). Surface charge reversal of typically positively charged iron oxide surface is likely the consequence of guanidine fragments of arginine complexing iron atoms at the surface with the remaining carboxylic group imparting overall negative charge upon ionization. We also found that the large excess of arginine is necessary to prepare the smallest particles and to assure uniform oxidation of magnetite to maghemite within 3-5 hours. The excess of arginine is likely important for interactions with AgNPs that is responsible for dragging them into the forming pellet.

The same charges of magnetic and plasmonic NPs (zeta potentials of -9 mV for maghemite NPs and -23 mV for citrate-stabilized AgJ_{13}NPs) are responsible for the hydrodynamic and weak electrostatic origin of the AgJ_{13}NP concentration rather than strong attractive electrostatic interaction of oppositely charged NPs. The weak electrostatic interactions are supported by slow flocculation of AgNPs and MHNPs which can be monitored by the solution colour (Fig. S3). These interactions dictate optimal aging time of AgJ_{13}NP&MH samples of 4-12 hours for SERS measurements. Arginine and PVP are two important components to control weak electrostatic interactions of AgNPs and MHNPs.

The hydrodynamic origin is also supported by the requirement of the minimal concentration of magnetic NPs to trap and drag AgNPs into the deposited layer. The hydrodynamic concentration is further corroborated by EM images (Figs. 1b and 1c) where no preferential adsorption of MHNPs to AgJ_{13}NPs is observed, as it would be the

case for the interaction of NPs with opposite charges. It is important to point out that TEM images do not representatively characterize the pellet, since EM measurements are performed upon drying and under high vacuum. For more AgJ_{13}NP and AgJ_{13}NP&MH TEM images see Figs. S4 and S5, respectively.

Lastly, the perchlorate salt of iron (II) was chosen as a precursor of magnetic nanoparticles instead of more common iron (II) chloride, since chloride is known to strongly affect silver NPs.[46]

Maghemite vs. magnetite. Considering that magnetite is the most commonly used material of magnetic NPs, direct comparison of magnetite and maghemite NPs was performed. Both maghemite and magnetite NPs were shown to be ca. 7.0 ± 1.3 nm in diameter by electron microscopy (see Fig. 1b and Fig. S6) and ca. 4.3 nm from PXRD data (Fig. S7), given the similarity of their preparations (see Experimental). It was determined that maghemite NPs offer superior enhancement compared to magnetite NPs at all analyte concentrations (Fig. 2a). The superior enhancement is primarily attributed to smaller optical absorption of maghemite dispersions in comparison to magnetite (Fig. 2c). The weaker optical absorption of maghemite originates from less charge transfer interactions, since maghemite is predominantly iron(III) oxide with the spinel structure retained.[47] Furthermore, AgJ_{13}NP&MH was found to yield a higher percent removal of AgNPs upon application of magnetic field, and thus efficiency of magnetic concentration than its magnetite analog (AgJ_{13}NP&MN), as shown in Figure 2d.

Optimal MH/Ag ratio, detection limits and reproducibility of measurements. The maghemite-to-silver ratio in AgJ_{13}NP&MH was explored to determine the best SERS enhancement in the system that is governed by the balance between optical clarity and ease of magnetic concentration. The optimal conditions were found to be the AgJ_{13}NP&MH with an iron-to-silver molar ratio of 1:1 (see Figs. S1 and S2). Subsequently, detection limits and reproducibility for this system were further investigated. The lower limit of detection was found to be 7.0 pM for DTNB. The key important feature of this system is high reproducibility for several consecutive trials: at concentrations (74 nM to 0.74 mM), the standard deviation of the signal peak intensity

for six random trials was below 10% (Fig. 1e). The formation of a uniform layer of Ag_{13}NPs on the inner side of the quartz cuvette, where the layer is smooth and stable, greatly enhances SERS detection reproducibility. The standard deviation of SERS signal for repeated re-dispersion and re-concentration cycles were similar ca. 10% at nanomolar concentrations. Near detection limits of 7.4 pM of DTNB, the reproducibility remained a respectable 40-60% (Fig. 1e.) The magnetic concentration of Ag_{13}NP by maghemite NPs enhanced the SERS signal consistently by a factor of 200 in a wide concentration range from mM to pM (Fig. 2a), with 1.19 log(counts) for Ag_{13}NP enhanced to 2.75 log(counts) for Ag_{13}NP&MH.

Ag_{13}NP compared to other plasmonic NPs in Ag&MH. The protocol for the formation of composite magnetic-plasmonic substrates developed for Ag_{13}NP&MH was subsequently extended to different types of gold and silver nanoparticles including gold-coated silver decahedra (Au@Ag_{13}NP&MH, with 10 mol. % Au relative to Ag),[48] silver pentagonal rods (AgPRNP&MH),[49,50] silver icosahedra (AgI_hNP&MH),[51] and stellated gold nanoparticles (AuStNP&MH). First, magnetic concentration with MHNPs works universally for all of the tested metal nanoparticles, since they all share in common charge stabilization of a negatively charged NP surface. At all analyte concentrations, the Ag_{13}NP&MH composites yielded the greatest enhancement of Raman signal (Figure 2b). The best enhancement for Ag_{13}NPs can be attributed to their sharp well-defined LSPR peaks with HWHM below 20 nm and a corresponding Q factor > 12, as well as their inability to pack into close packed arrays due to their pentagonal symmetry[43] that creates consistent interparticle gaps advantageous for SERS.[52,53]

CONCLUSIONS

With the excellent reproducibility of measurements due to the creation of uniform SERS “hot spots”, picomolar detection limits, and simple preparation including an option of using PMMA sample cells, the developed nanocomposite Ag&MH substrate offers great promise for SERS and will be further optimized for specific applications.

ACKNOWLEDGMENTS

The authors would like to thank NSERC and the Government of Ontario (ERA Award) for funding; Nathan Henderson (Bruker AXS Inc., Madison, WI) for performing PRXD measurements and data analysis; Ilya Gourevich and Neil Coombs (Centre for Nanostructure Imaging, University of Toronto) for the support and assistance with electron microscopy imaging.

TOC image:

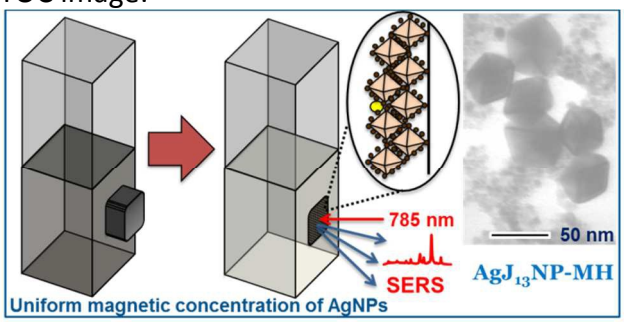

TOC text:

Same-charge maghemite NPs act as a hydrodynamic net to concentrate SERS active AgJ_{13}NPs, enabling uniform “hot spots” and reproducible Raman detection of low analyte concentrations.

FIGURES & CAPTIONS

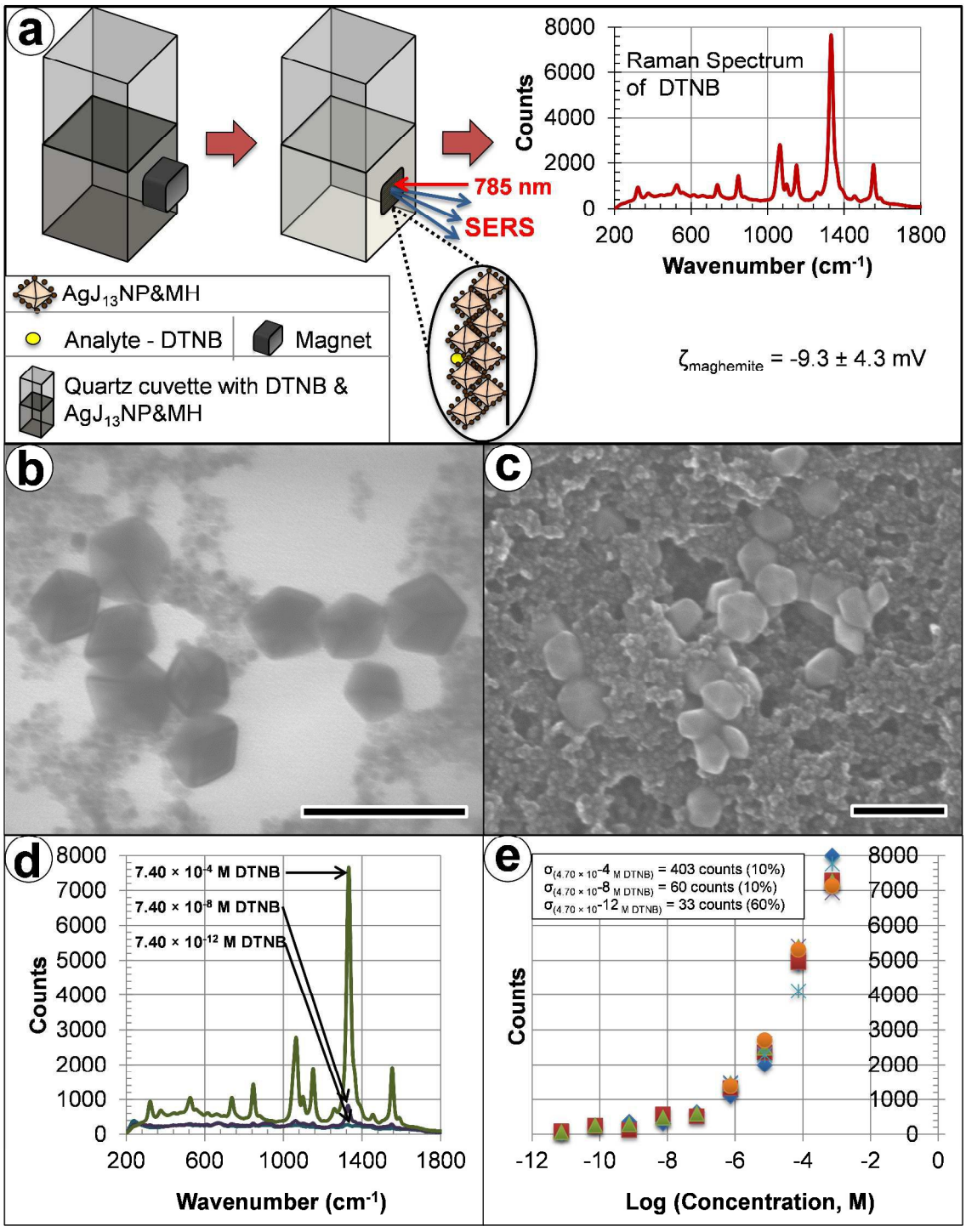

Figure 1. (a) Schematic representation of SERS measurements using the developed Ag&MH nanocomposite substrate. **(b)** TEM and **(c)** SEM images of AgJ_{13}NP&MH; scale bars are 100 nm. **(d)** Series of SERS spectra of DTNB detection by AgJ_{13}NP&MH at DTNB

concentrations ranging from 7.40 pM to 0.740 mM. **(e)** Reproducibility and reliability of multiple measurements both at different spots of the same substrate and after several cycles of AgJ_{13}NP&MH re-dispersion and re-concentration.

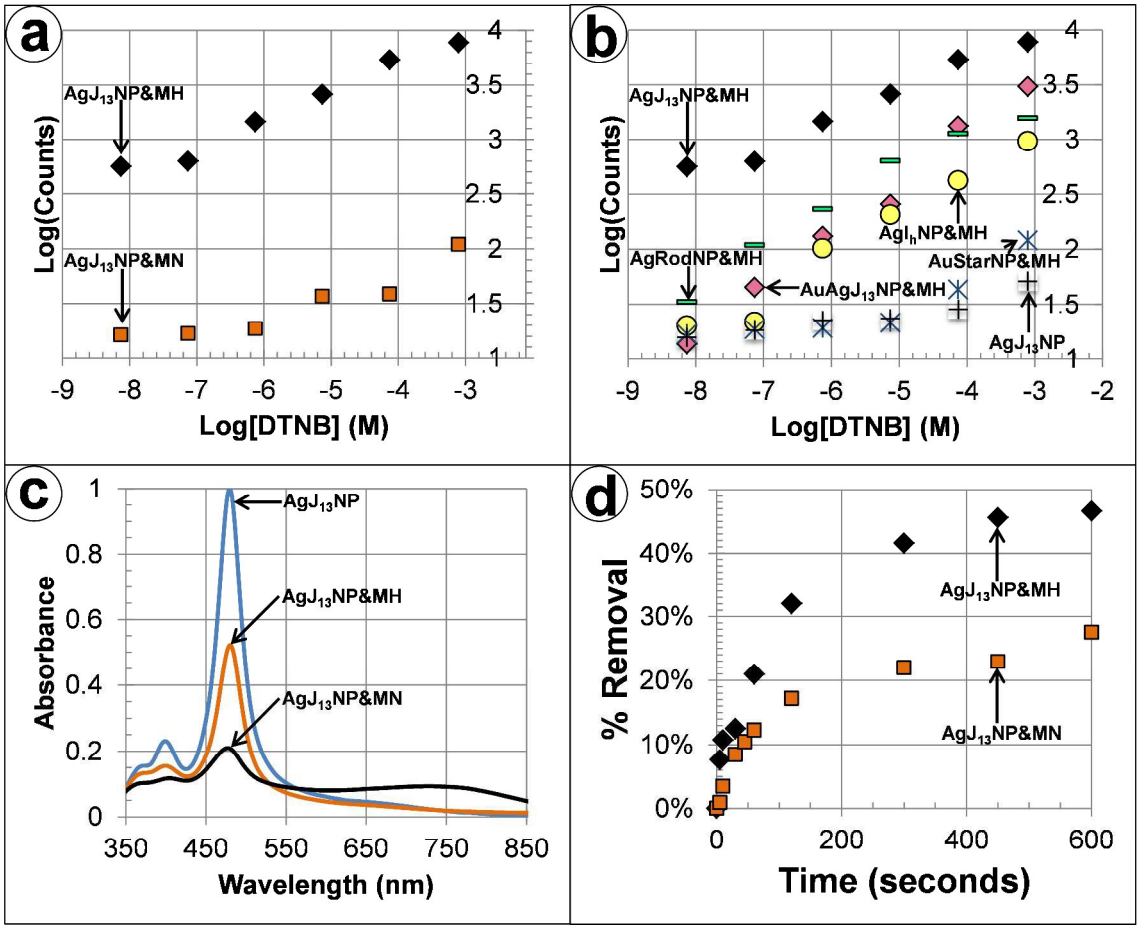

Figure 2. Comparison of SERS detection sensitivity of DTNB: (a) between AgJ_{13}NP&MH and AgJ_{13}NP&MN; (b) between AgJ_{13}NP&MH and various plasmonic nanoparticles concentrated by maghemite (see full description in the text). For both (a) and (b) the DTNB concentration varied from 7.40×10^{-9} M to 7.87×10^{-4} M. (c) Normalized UV-vis spectra of AgJ_{13}NP, AgJ_{13}NP&MN and AgJ_{13}NP&MH. (d) Percentage of magnetic removal of AgJ_{13}NPs with time for 1:1 Ag to Fe AgJ_{13}NP&MH and 1:5 Ag to Fe AgJ_{13}NP&MN.

REFERENCES

[1] G. Baffou and R. Quidant, Nanoplasmonics for chemistry. *Chem. Soc. Rev.* 2014, **43**, 3898–3907.
[2] P. D. Howes, R. Subinoy and M. M. Stevens, Plasmonic nanomaterials for biodiagnostics. *Chem. Soc. Rev.* 2014, **43**, 3835–3853.
[3] J. J. Giner-Casares and L. M. Liz-Marzan, Plasmonic nanoparticles in 2D for biological applications: Toward active multipurpose platforms. *Nano Today* 2014, **9**, 365–377.
[4] A. M. Alkilany, S. E. Lohse and C. J. Murphy, The Gold Standard: Gold Nanoparticle Libraries To Understand the Nano-Bio Interface. *Acc. Chem. Res.* 2013, **46**, 650–661.
[5] S. Szunerits and R. Boukherroub, Sensing using localised surface plasmon resonance sensors. *Chem. Commun.* 2012, **48**, 8999–9010.
[6] S. Lal, N. K. Grady, J. Kundu, C. S. Levin, J. B. Lassiter and N. J. Halas, Tailoring plasmonic substrates for surface enhanced spectroscopies. *Chem. Soc. Rev.* 2008, **37**, 898–911.
[7] X-C. Chen, G. Cabello, D-Y. Wu and Z-Q. Tian, Surface-enhanced Raman spectroscopy toward application in plasmonic photocatalysis on metal nanostructures. *J. Photochem. Photobiol. C*: 2014, **21**, 54–80.
[8] J. Kneipp, H. Kniepp and K. Kniepp, SERS—a single-molecule and nanoscale tool for bioanalytics. *Chem. Soc. Rev.* 2008, **37**, 1052–1060.
[9] A. Pallaoro, M. R. Hoonejani, G. B. Braun, C. D. Meinhart and M. Moskovits, Rapid Identification by Surface-Enhanced Raman Spectroscopy of Cancer Cells at Low Concentrations Flowing in a Microfluidic Channel. *ACS Nano* 2015, **9**, 4328–4336.
[10] N. E. Motl, A. F. Smith, C. J. DeSantis and S. E. Skrabalak, Engineering plasmonic metal colloids through composition and structural design. *Chem. Soc. Rev.* 2014, **43**, 3823–3834.
[11] R. A. Sperling, P. R. Gil, F. Zhang, M. Zanella and W. J. Parak, Biological applications of gold nanoparticles. *Chem. Soc. Rev.* 2008, **37**, 1896–1908.
[12] S. Schluecker, Surface-Enhanced Raman Spectroscopy: Concepts and Chemical Applications. *Angew. Chemie Int. Ed.* 2014, **53**, 4756–4795.
[13] J. F. Betz, W. W. Yu, Y. Cheng, I. M. White and G. W. Rubloff, Simple SERS substrates: powerful, portable, and full of potential. Surface-Enhanced Raman Spectroscopy: Concepts and Chemical Applications. *Phys. Chem. Chem. Phys.* 2014, **16**, 2224–2239.
[14] M. Moskovits, Surface-enhanced spectroscopy. *Rev. Mod. Phys.* 1985, **57**, 783–826.
[15] M. D. Sonntag, J. M. Klingsporn, A. B. Zrimsek, B. Sharma, L. K. Ruvuna and R. P. Van Duyne, Molecular plasmonics for nanoscale spectroscopy. *Chem. Soc. Rev.* 2014, **43**, 1230–1247.
[16] M. Fleischmann, P. J. Hendra and A. J. McQuillan, Raman spectra from electrode surfaces. *J. Chem. Soc., Chem. Commun.* 1973, **3**, 80–81.
[17] X. Li, L. Wang and C. Li, Rolling-Circle Amplification Detection of Thrombin Using Surface-Enhanced Raman Spectroscopy with Core-Shell Nanoparticle Probe. *Chem. Eur. J.* 2015, **18**, 6817–6822.
[18] J. Lima and S. A. Majetich, Composite magnetic—plasmonic nanoparticles forbiomedicine: Manipulation and imaging. *Nano Today* 2013, **8**, 98–113.
[19] M. Gühlke, S. Selve and J. Kneipp, Magnetic separation and SERS observation of analyte molecules on bifunctional silver/iron oxide composite nanostructures. *J. Raman Spectrosc.* 2012, **43**, 1204–1207.
[20] Y. M. Zhai, J. F. Zhai, Y. L. Wang, S. J. Guo, W. Ren and S. J. Dong, Fabrication of Iron Oxide Core/Gold Shell Submicrometer Spheres with Nanoscale Surface Roughness for Efficient Surface-Enhanced Raman Scattering. *J. Phys. Chem. C* 2009, **113**, 7009–7014.

[21] J. H. Gao, H. W. Gu and B. Xu, Multifunctional Magnetic Nanoparticles: Design, Synthesis, and Biomedical Applications. *Acc. Chem. Res.* 2009, **42**, 1097–1107.
[22] G. L. Liu, Y. Lu, J. Kim, J. C. Doll and L. P. Lee, Magnetic Nanocrescents as Controllable Surface-Enhanced Raman Scattering Nanoprobes for Biomolecular Imaging. *Adv. Mater*. 2005, **17**, 2683–2688.
[23] K. Kim, J. Y. Choi, H. B. Lee and K. S. Shin, Silanization of Ag-Deposited Magnetite Particles: An Efficient Route to Fabricate Magnetic Nanoparticle-Based Raman Barcode Materials. *ACS Appl. Mater. Interfaces.* 2010, **2**, 1872–1878.
[24] B. H. Jun, M. S. Noh, J. Kim, G. Kim, H. Kang, M. S. Kim, Y. T. Seo, J. Baek, J. H. Kim, J. Park, S. Kim, Y. K. Kim, T. Hyeon, M. H. Cho, D. H. Jeong and Y. S. Lee, Multifunctional Silver-Embedded Magnetic Nanoparticles as SERS Nanoprobes and Their Applications. *Small* 2010, **6**, 119–125.
[25] B. H. Jun, M. S. Noh, J. Kim, G. Kim, H. Kang, J. H. Kim, W. J. Chung, M. S. Kim, Y. K. Kim, M. H. Cho, D. H. Jeong and Y. S. Lee, Protein separation and identification using magnetic beads encoded with surface-enhanced Raman spectroscopy. *Anal. Biochem.* 2009, **391**, 24–30.
[26] T. Donnelly, W. E. Smith, K. Faulds and D. Graham, Silver and magnetic nanoparticles for sensitive DNA detection by SERS. *Chem. Commun.* 2014, **50**, 12907–12910.
[27] S. A. Chen, Y. X. Yuan, J. L. Yao, S. Y. Han and R. A. Gu, Magnetic separation and immunoassay of multi-antigen based on surface enhanced Raman spectroscopy. *Chem. Commun.* 2011, **47**, 4225–4227.
[28] B. Guven, N. Basaran-Akgul, E. Temur, U. Tamer and I. H. Boyaci, SERS-based sandwich immunoassay using antibody coated magnetic nanoparticles for Escherichia coli enumeration. *Analyst* 2011, **136**, 740–748.
[29] F. Bao, J. L. Yao and R. A. Gu, Synthesis of magnetic Fe_2O_3/Au core/shell nanoparticles for bioseparation and immunoassay based on surface-enhanced Raman spectroscopy. *Langmuir* 2009, **25**, 10782-10787.
[30] H; Zhang and M. E. Meyerhoff, Gold-coated magnetic particles for solid-phase immunoassays: enhancing immobilized antibody binding efficiency and analytical performance. *Anal. Chem.* 2006, **78**, 609-616.
[31] R. Contreras-Caceres, S. Abalde-Cela, P. Guardia-Giros, A. Fernandez-Barbero, J. Perez-Juste, R. A. Alvarez-Puebla, L. M. Liz-Marzan, Multifunctional microgel magnetic/optical traps for SERS ultradetection. *Langmuir* 2011, **27**, 4520-4525.
[32] M. Spuch-Calvar, L. Rodriguez-Lorenzo, M. P. Morales, R. A. Alvarez-Puebla and L. M. Liz-Marzan, Bifunctional nanocomposites with long-term stability, as SERS optical accumulators for ultrasensitive analysis. *J. Phys. Chem. C* 2009, **113**, 3373-3377.
[33] Q. An, P. Zhang, J. M. Li, W. F. Ma, J. Guo, J. Hu and C. C. Wang, Silver-coated magnetite–carbon core–shell microspheres as substrate-enhanced SERS probes for detection of trace persistent organic pollutants. *Nanoscale* 2012, **4**, 5210–5216.
[34] D. Jana, A. Mandal and G. De, High Raman Enhancing Shape-Tunable Ag Nanoplates in Alumina: A Reliable and Efficient SERS Technique. *ACS Appl. Mater. Interfaces* 2012, **4**, 3330−3334.
[35] M. Kaya and M. Volkan, New Approach for the Surface Enhanced Resonance Raman Scattering (SERRS) Detection of Dopamine at Picomolar (pM) Levels in the Presence of Ascorbic Acid. *Anal. Chem.* 2012, **84**, 7729−7735.
[36] K. A. Mahmound and M. Zourob, Fe_3O_4/Au nanoparticles/lignin modified microspheres as effectual surface enhanced Raman scattering (SERS) substrates for highly selective and sensitive detection of 2,4,6-trinitrotoluene (TNT). *Analyst* 2013, **138**, 2712–2719.

[37] Z. Y. Bao, J. Dai, D. Y. Lei and Y. Wu, Maximizing surface-enhanced Raman scattering sensitivity of surfactant-free Ag-Fe_3O_4nanocomposites through optimization of silver nanoparticle density and magnetic self-assembly. *J. Appl. Phys*. 2013, **114**, 124305.
[38] K. Kim, H. J. Jang and K. S. Shin, Ag nanostructures assembled on magnetic particles for ready SERS-based detection of dissolved chemical species. *Analyst* 2009, **134**, 308–313.
[39] M. F. Zhang, A. W. Zhao, D. P. Wang and H. H. Sun, Hierarchically assembled NiCo@SiO_2@Ag magnetic core-shell microspheres as highly efficient and recyclable 3D SERS substrates. *Analyst* 2015, **140**, 440–448.
[40] A. Shiohara, Y. Wang, L. M. Liz-Marzan, Recent approaches toward creation of hot spots for SERS detection. *J. Photochem. Photobiol. C*: 2014, **21**, 2–25.
[41] K. A. Willets, Super-resolution imaging of SERS hot spots. *Chem. Soc. Rev.* 2014, **43**, 3854–3864.
[42] M. Moskovits, Persistent misconceptions regarding SERS. *Phys. Chem. Chem. Phys.* 2013, **15**, 5301–5311.
[43] B. Pietrobon, and V. Kitaev, Photochemical Synthesis of Monodisperse Size-Controlled Silver Decahedral Nanoparticles and Their Remarkable Optical Properties. *Chem. Mater.* 2008, **20**, 5186–5190.
[44] Z. Wang, H. Zhu, X. Wang, F. Yang and X. Yang, One-pot green synthesis of biocompatible arginine-stabilized magnetic nanoparticles. *Nanotechnology* 2009, **20**, 465606.
[45] I. S. Smolkova, N. E. Kazantseva, V. Babayan, P. Smolka, H. Parmar, J. Vilcakova, O. Schneeweiss, N. Pizurova, Alternating magnetic field energy absorption in the dispersion of iron oxide nanoparticles in a viscous medium. *J. of Magnetism and Magnetic Materials* 2015, **374**, 508–515.
[46] N. Cathcart, A. J. Frank and V. Kitaev, Silver nanoparticles with planar twinned defects: effect of halides for precise tuning of plasmon resonance maxima from 400 to >900 nm. *Chem. Commun.* 2009, **46**, 7170–7172.
[47] D. Carta, A. Corrias, A. Falqui, R. Brescia, E. Fantechi, F. Pineider and C. Sangregorio, EDS, HRTEM/STEM, and X-ray Absorption Spectroscopy Studies of Co-Substituted Maghemite Nanoparticles. *J. Phys. Chem. C* 2013, *117*, 9496–9506.
[48] N. Murshid, I. Gourevich, N. Coombs and V. Kitaev, Gold Plating of Silver Nanoparticles for Superior Stability and Preserved Plasmonic and Sensing Properties. *Chem. Commun.* 2013, **49***,* 11355–11357.
[49] N. Murshid, D. Keogh and V. Kitaev, Optimized Synthetic Protocols for Preparation of Versatile Plasmonic Platform Based on Silver Nanoparticles with Pentagonal Symmetries. *Part. Part. Syst. Charact.* 2014, **31***,* 178–189.
[50] B. Pietrobon, M. McEachran and V. Kitaev, Synthesis of Size-Controlled Faceted Pentagonal Silver Nanorods with Tunable Plasmonic Properties and Self-Assembly of These Nanorods. *ACS Nano* 2009, **3**, 21–26.
[51] R. A. Keunen, N. Cathcart and V. Kitaev, Plasmon Mediated Shape and Size Selective Synthesis of Icosahedral Silver Nanoparticles via Oxidative Etching and Their 1-D Transformation to Pentagonal Pins. *Nanoscale* 2014, **6**, 8045–8051.
[52] T. Ding, L. O. Herrmann, B. de Nijs, F. Benz and J. J. Baumberg, Self-Aligned Colloidal Lithography for Controllable and Tuneable Plasmonic Nanogaps. *Small* 2015, **11**, 2139–2143.
[53] J. C. Fraire, V. N. S. Ocello, L. G. Allende, A. V. Veglia and E. A. Coronado, Toward the Design of Highly Stable Small Colloidal SERS Substrates with Supramolecular Host-Guest Interactions for Ultrasensitive Detection. *J. Phys. Chem. C* 2015, **119**, 8876–8888.